Journal of Solid State Chemistry 212 (2014) 114–120

Contents lists available at ScienceDirect

Journal of Solid State Chemistry

journal homepage: www.elsevier.com/locate/jssc

Crystal structure and magnetic properties of titanium-based $CuTi_{2-x}M_xS_4$ and $CuCr_{2-x}Ti_xSe_4$ chalcospinels

P. Barahona [a,**], A. Galdámez [b,*], F. López-Vergara [b], V. Manríquez [b], O. Peña [c]

[a] Facultad de Ciencias Básicas, Universidad Católica del Maule, Talca, Chile
[b] Departamento de Química, Facultad de Ciencias, Universidad de Chile, Santiago, Chile
[c] Institut des Sciences Chimiques de Rennes, UMR 6226, Université de Rennes 1, Rennes, France

ARTICLE INFO

Article history:
Received 23 September 2013
Received in revised form
10 January 2014
Accepted 13 January 2014
Available online 23 January 2014

Keywords:
Chalcospinel
Crystal structure
Magnetic properties

ABSTRACT

$CuTi_{2-x}M_xS_4$ (M=Fe, Mn, Co; x=0.3, 0.5) and $CuCr_{2-x}Ti_xSe_4$ (x=0.3, 0.5, 0.7) chalcospinels were synthesized by conventional solid-state reactions. Their crystal structures were determined by single-crystal X-ray diffraction. All of the phases crystallized in cubic spinel-type structures (space group, $Fd\bar{3}m$). For all of the chalcospinel compounds, the edge-length distortion parameter (ELD) indicated that the most distorted polyhedron was $Q[(Ti,M)_3Cu]$, which displayed an ~8% distortion from an ideal tetrahedron structure (Q=S or Se).

The Mn-based thiospinel $CuMn_{0.3}Ti_{1.7}S_4$ is paramagnetic, whereas the Fe-based thiospinels ($CuTi_{2-x}Fe_xS_4$; x=0.3 and 0.7) are strongly antiferromagnetic due to their spin-glass states. The magnetic susceptibility measurements indicated ferromagnetic behavior for the selenospinels ($CuCr_{2-x}Ti_xSe_4$; x=0.3, 0.5 and 0.7).

© 2014 Elsevier Inc. All rights reserved.

1. Introduction

It is well known that seleno- and thiospinels, such as $CuCr_2Q_4$ (Q=S, Se), $Cu_{0.5}Co_{0.5}Cr_2Se_4$, $Cu(Cr_xTi_{1-x})_2S_4$, $Cu_2CoTi_xSn_{3-x}S_8$ (or $CuCo_{0.5}Ti_{x/2}Sn_{(3-x)/2}S_4$) and $CuTi_2S_4$, have many interesting magnetic, thermoelectric, electrochemical and optical properties [1–9]. The spinel structure of CuM_2Q_4 (Q=S, Se) presents the M cations in octahedral sites (16*d*) and Cu cations at its tetrahedral sites (8*a*). The unit cell contains Q anions (bonded to one Cu and three M cations) in a cubic close-packing arrangement (32*e* site). Spinel $CuTi_2S_4$ is a metallic conductor that shows a paramagnetic behavior, whereas $CuCr_2Se_4$ is a ferromagnetic metal spinel with a high Curie temperature (~430 K) [5,10].

Kleinke et al. suggested that the Cu^+ copper cations in the $CuTi_2S_4$ spinel structure are located at the 8*a* tetrahedral sites, while the Ti^{3+} and Ti^{4+} titanium ions are located at the 16*d* octahedral sites [11]. Recently, Parasyuk et al. synthesized new $Cu_2MTi_3S_8$ (or $CuM_{0.5}Ti_{1.5}S_4$) thiospinels by substituting Ti for Mn or Ni [12]. $Cu_2FeTi_3S_8$ (or $CuFe_{0.5}Ti_{1.5}S_4$) and $CuCr_2Se_4$ have been used as an Fe(III)-selective electrode material or as an electrode material in lithium cells [13–16]. The magnetic phase diagram of $Cu(Cr_xTi_{1-x})_2S_4$ was established experimentally by Nagata et al. [4]. The authors suggested that the evolution from the ferromagnetic regime to the spin-glass regime was caused by magnetic frustrations triggered by the titanium substitutions.

Electronic state models for $CuCr_2Se_4$ have been proposed by Lotgering and Goodenough [17,18]. Lotgering et al. explained the properties of $CuCr_2Se_4$ by assuming that the charge distribution could be represented by $Cu^+[Cr^{3+}Cr^{4+}]Se_4^{2-}$, in which the metallic conduction and ferromagnetism are attributed to the double exchange between Cr^{3+} and Cr^{4+}. In contrast, Goodenough suggested a model that can be described by the formula $Cu^{2+}[Cr^{3+}]_2Se_4^{2-}$. Soft X-ray absorption spectroscopy (XAS) and magnetic circular dichroism (XMCD) analyses of $CuCr_xTi_{2-x}Se_4$ selenospinels revealed that the oxidation state changes from Cu^+ to Cu^{2+} (for increasing x), whereas the titanium atoms exist in the 4+ oxidation state [19]. Thus, the oxidation states of the cations play an important role in the peculiar magnetic/electrical properties of these compounds.

The present work describes the synthesis and characterization of the $CuTi_{1.7}Mn_{0.3}S_4$, $CuTi_{1.7}Fe_{0.3}S_4$, $CuTi_{1.5}Fe_{0.5}S_4$, $CuTi_{1.7}Co_{0.3}S_4$, $CuTi_{1.5}Co_{0.5}S_4$, $CuCr_{1.3}Ti_{0.7}Se_4$, $CuCr_{1.5}Ti_{0.5}Se_4$ and $CuCr_{1.5}Ti_{0.5}Se_4$ phases. Our goal was to determine the influence of chemical substitution on the crystal structure and magnetic properties of these compounds.

2. Experimental

2.1. Synthesis

Polycrystalline compounds were prepared by directly combining high-purity elemental powders (99.99%, Aldrich) in stoichiometric amounts. All manipulations were carried out under an

* Corresponding author. Tel.: +56 2 978 7267; fax: +56 2 271 3888.
** Corresponding author.
E-mail addresses: pbaraho@ucm.cl (P. Barahona), agaldamez@uchile.cl (A. Galdámez).

0022-4596/$ - see front matter © 2014 Elsevier Inc. All rights reserved.
http://dx.doi.org/10.1016/j.jssc.2014.01.017

argon atmosphere. The reaction mixtures were pressed into round-shaped pellets (6 mm in diameter), sealed in evacuated quartz ampoules and placed in a programmable furnace. The ampoules were then slowly heated from room temperature to 850 °C at a rate of 1 °C/min and held at the maximum temperature for 6 days. Finally, the ampoules were slowly cooled from 850 °C to room temperature at a rate of 1 °C/min.

2.2. Crystal structure determination

XRD data for all of the selected single crystals were collected at room temperature using a Bruker Kappa CCD diffractometer with graphite-monochromatized *MoKα* radiation (λ=0.71073 Å). The intensity data were collected using the COLLECT program [20]. Cell refinement and data reduction were performed with the Dirax/lsq and EvalCCD programs [21,22]. The crystal structures were refined in a least-squares full matrix using the SHELXL package of crystallographic programs [23]. The refined occupation factors of Fe, Mn, Co, Cr and Ti were consistent with the energy-dispersive X-ray chemical analyses EDAX on the seven single crystals used for X-ray diffraction measurements. The CIF files were deposited in the FIZ Karlsruhe database (76344 Eggenstein-Leopoldshafen, Germany; e-mail: crysdata@fiz-karlsruhe.de; fax: (49)7247-808-666). The depository numbers are CSD-426370 for $CuTi_{1.7}Mn_{0.3}S_4$, CSD-426371 for $CuTi_{1.7}Fe_{0.3}S_4$, CSD-426372 for $CuTi_{1.5}Fe_{0.5}S_4$, CSD-426373 for $CuTi_{1.7}Co_{0.3}S_4$, CSD-426374 for $CuTi_{1.5}Co_{0.5}S_4$, CSD-426375 for $CuCr_{1.3}Ti_{0.7}Se_4$ and CSD-426376 for $CuCr_{1.5}Ti_{0.5}Se_4$.

2.3. SEM-EDAX analysis

The chemical compositions of the single crystals and powder samples were determined by scanning electron microscopy with the aid of energy-dispersive X-ray analysis (SEM-EDAX) using a JEOL 5400 system equipped with an Oxford Link ISIS microanalyzer. The working distance was 35 mm and the accelerating voltage was 22.5 kV. The samples were mounted on double-sided carbon tape, which adhered to an aluminum specimen holder. The EDAX spectra were collected for 60 s.

2.4. Powder X-ray diffraction

Powder XRD patterns were collected at room temperature using a Siemens D5000 powder diffractometer, with Cu*Kα* radiation (λ=1.541871 Å) in the range of $5^\circ < 2\theta < 80^\circ$. The XRD patterns were indexed using the CHECKCELL program.

2.5. Magnetic measurements

Magnetic measurements were performed on pelletized powder samples using a Quantum Design MPMS XL5 SQUID susceptometer. Two kinds of experiments were performed. First, the ferro(ferri) magnetic nature of the material was determined using ZFC/FC (zero-field-cooled/field-cooled) cycles at low fields (typically 0.5 to 1 kOe). Second, the effective paramagnetic moments were evaluated from susceptibility measurements at high temperatures (well above the magnetic transition temperature) and high applied fields (H_{app}=10 kOe). Additional experiments were performed in the case of Fe-doped samples in order to study their spin-glass nature; for this, a.c. susceptibility was measured at low temperatures as a function of frequency in the range [1 Hz–1 kHz]. In all cases, the experimental data was corrected by the core diamagnetic contribution of the constituent atoms.

3. Results and discussion

3.1. Crystal structure

The crystal structures for seven single crystals of $CuTi_{2-x}M_xS_4$ (M=Fe, Mn, Co; x=0.3, 0.5) and $CuCr_{2-x}Ti_xSe_4$ (x=0.5, 0.7) were resolved by XRD. All of the crystals were in the space group $Fd\bar{3}m$, corresponding to spinel-type structures. The least-squares refinement of the occupation factors and the displacement parameters converged to a model in which the tetrahedral positions were occupied by Cu (8*a* sites) and the octahedral positions (16*d* sites) were occupied by Ti, *M* and Cr. The S or Se atoms occupy the 32*e* (*u*,*u*,*u*) sites in a cubic closed-packed array. The refined occupation factors of the octahedral sites were $16d=(2-x)$ Ti$+x$ *M* in the

Table 1
Crystallographic data and structure refinement details for $CuTi_{1.7}Mn_{0.3}S_4$(**I**), $CuTi_{1.7}Fe_{0.3}S_4$(**II**), $CuTi_{1.5}Fe_{0.5}S_4$(**III**).

Compound	(**I**)	(**II**)	(**III**)
Crystal data			
Crystal system, space group	Cubic, *Fd*-3*m*		
Unit cell dimension *a* (Å)	10.0535(12)	10.0005(12)	10.0131(12)
Cell volume (Å^3)	1016.1(2)	1000.1(2)	1003.9(2)
Data collection			
Temperature (K)	293(2)		
Wavelength (*Mo Kα*)	0.71073 Å		
Equipment	Kappa CCD		
Absorption coefficient (mm^{-1})	4.798	5.062	5.043
θ-range (°)	$3.51 < \theta < 41.83$	$3.53 < \theta < 29.83$	$3.52 < \theta < 41.97$
hkl-range	$-18 \le h \le 13$ $-15 \le k \le 18$ $-17 \le l \le 18$	$-14 \le h \le 11$ $-12 \le k \le 14$ $-13 \le l \le 13$	$-15 \le h \le 18$ $-13 \le k \le 14$ $-18 \le l \le 18$
No. of reflections	3691	1973	3649
$R_{int.}$, R_σ	0.0329, 0.0133	0.0338, 0.0113	0.0333, 0.0139
No. of independent reflections	203	91	200
Refinement			
Refinement method	Full-matrix least-squares on F^2		
No. of parameters	10	10	10
Extinction coefficient	0.0016(2)	0.0016(3)	0.0039(4)
R ($I > 2\sigma_I$), R (all)	0.0241, 0.0305	0.0239, 0.0274	0.0219, 0.0261
$wR2$ ($I > 2\sigma_I$), $wR2$ (all)	0.0546, 0.0575	0.0658, 0.0693	0.0563, 0.0636
GooF=S	0.815	1.278	0.889
Largest diff. peaks (e Å^{-3})	0.688, −0.598	0.542, −0.963	1.537, −0.939

Table 2
Crystallographic data and structure refinement details for $CuTi_{1.7}Co_{0.3}S_4$(**IV**), $CuTi_{1.5}Co_{0.5}S_4$(**V**), $CuCr_{1.3}Ti_{0.7}Se_4$(**VI**), and $CuCr_{1.5}Ti_{0.5}Se_4$(**VII**).

Compound	(**IV**)	(**V**)	(**VI**)	(**VII**)
Crystal data				
Crystal system, space group	Cubic, *Fd*-3*m*			
Lattice constants (Å)	9.9352(11)	9.8852(11)	10.4165(12)	10.4009(12)
Cell volume (Å^3)	980.69(19)	965.95(19)	1130.2(2)	1125.2(2)
Data collection				
Temperature (K)	293(2)			
Wavelength (*Mo* Kα)	0.71073 Å			
Equipment	Kappa CCD			
Absorption coefficient (mm^{-1})	5.375	5.457	16.301	16.375
θ-range/°	$5.55 < \theta < 32.67$	$3.57 < \theta < 41.82$	$5.54 < \theta < 41.95$	$5.55 < \theta < 41.69$
hkl-range	$-14 \le h \le 13$ $-14 \le k \le 10$ $-12 \le l \le 14$	$-11 \le h \le 17$ $-18 \le k \le 7$ $-16 \le l \le 17$	$-14 \le h \le 16$ $-17 \le k \le 19$ $-19 \le l \le 19$	$-17 \le h \le 18$ $-19 \le k \le 19$ $-18 \le l \le 13$
No. of reflections,	1576	2483	2914	2809
$R_{int.}$, R_σ	0.0409, 0.0163	0.0439, 0.0202	0.0441, 0.0189	0.0411, 0.0201
No. independent reflections	109	193	220	219
Refinement				
Refinement method	Full-matrix least-squares on F^2			
No. of parameters	10	10	8	8
Extinction coefficient	0.0001(3)	0.0010(4)	0.0335	0.00101(9)
R ($I > 2\sigma_I$), R (all)	0.0330, 0.0396	0.0327, 0.0555	0.0226, 0.0335	0.0281, 0.0389
$wR2$ ($I > 2\sigma_I$), $wR2$ (all)	0.0861, 0.0901	0.0810, 0.0953	0.0542,0.0556	0.0516, 0.0540
GooF=S	1.247	1.145	1.250	1.207
Largest diff. peaks (e Å^{-3})	1.482, −1.357	1.914, −0.964	1.717, −1.212	2.089, −1.900

Table 3
Anionic *u* parameters and equivalent isotropic displacement parameters.

Compound	Anion *u* parameter	U_{eq} (Å^2)		
		Cu	Metal/Ti	Q=S or Se
$CuTi_{1.7}Mn_{0.3}S_4$	0.25557(4)	0.01316(17)	0.01314(15)	0.01229(16)
$CuTi_{1.7}Fe_{0.3}S_4$	0.25538(8)	0.0151(5)	0.0132(5)	0.0095(4)
$CuTi_{1.5}Fe_{0.5}S_4$	0.25570(3)	0.01308(17)	0.01453(16)	0.01014(15)
$CuTi_{1.7}Co_{0.3}S_4$	0.25575(9)	0.0196(6)	0.0139(5)	0.0123(4)
$CuTi_{1.5}Co_{0.5}S_4$	0.25634(6)	0.0217(3)	0.0150(3)	0.0148(3)
$CuCr_{1.3}Ti_{0.7}Se_4$	0.25575(9)	0.0144(2)	0.01014(18)	0.00900(12)
$CuCr_{1.5}Ti_{0.5}Se_4$	0.25665(2)	0.0137(2)	0.00985(19)	0.00913(13)

U_{eq} is defined as one third of the trace of the orthogonalized U_{ij} tensor.
Cu in A site (8*a*); Metal/Ti in B site (16*d*) and *Q* in Anion site (32*e*).

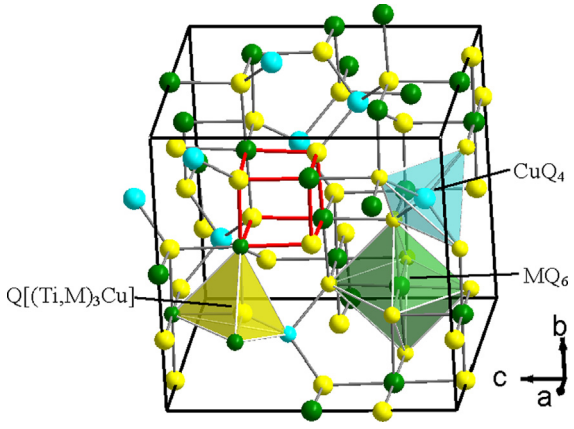

Fig. 1. Crystal structure of chalcospinels with chemical formula: Cu(*M*,Ti)$_2Q_4$ (*Q*=S or Se). The solid lines indicate the polyhedral network structure. The copper (cyan) is coordinated tetrahedrally by the chalcogen *Q* atoms. The metals (green) randomly occupy the 16*d* crystallographic sites and are coordinated octahedrally by the *Q* atoms. The metals surrounding the chalcogen *Q* (yellow) constitute a *Q*[(Ti, *M*)$_3$Cu] tetrahedron.

thiospinels and 16*d*=(2−*x*) Cr+*x*Ti in the selenospinels. The Ti, *M* and Cr atoms were constrained to have identical displacement parameters. Anisotropic thermal parameter refinements were applied to all of the atoms. The detailed crystallographic data and refinement results for all of the single crystals are summarized in Tables 1 and 2. The atomic coordinates and equivalent isotropic displacement parameters are listed in Table 3.

The $CuTi_{1.7}Mn_{0.3}S_4$(**I**), $CuTi_{1.7}Fe_{0.3}S_4$(**II**), $CuTi_{1.5}Fe_{0.5}S_4$(**III**), $CuTi_{1.7}Co_{0.3}S_4$(**IV**), $CuTi_{1.5}Co_{0.5}S_4$(**V**), $CuCr_{1.3}Ti_{0.7}Se_4$(**VI**) and $CuCr_{1.5}Ti_{0.5}Se_4$(**VII**) samples were isostructural and adopted spinel-type structures. The main features in the crystal structure are the tetrahedral CuQ_4 and the octahedral MQ_6 polyhedron. The Cu–S distances in the thiospinels ranged from 2.2583(14) to 2.2737(8) Å, and the Cu–Se distances in the selenospinels ranged from 2.37010(5) to 2.3716(5) Å. The Cu–S distances were close to the tetrahedral covalent radii evaluated by Pyykkö (Cu–S: 2.313 Å) [24]. These distances were also consistent with the bond lengths of cubic $CuTi_2S_4$ (2.2573 Å), rhombohedral $CuTi_2S_4$ (2.243 to 2.284 Å) and $Cu_{7.38(11)}Mn_4Sn_{12}S_{32}$ (2.3315 Å) [11,25]. The octahedral MQ_6 contained mixed metals that caused distortions in the chalcogen sub-lattice (see below). The *M*–S bond distances in **I**, **II**, **III**, **IV** and **V** (2.4102 to 2.4586 Å) were consistent with the bond lengths for cubic $CuTi_2S_4$ (Ti–S: 2.4501 Å), $Cu_2MnTi_3S_8$ (Mn/Ti–S: 2.450 Å), $Cu_{7.38(11)}Mn_4Sn_{12}S_{32}$ (Mn/Sn–S: 2.5601 Å) and $Cu_{5.47}Fe_{2.9}Sn_{13.1}S_{32}$ (Fe/Sn–S: 2.5419 Å) [11,12,25,26]. The (Cr/Ti)–Se bond distances in **VI** and **VII** (2.5390(4) Å and 2.5330 (4) Å) were consistent with the (Cr/In)–Se bond length (2.5541(3) Å) of $CdCr_{1.81}In_{0.19}Se_4$ [27].

The degrees of distortion of the tetrahedra or octahedra were evaluated using the distortion indices (DI) defined by Baur and Wildner [28–30]. The $CuTi_{2-x}M_xS_4$ and $CuCr_{2-x}Ti_xSe_4$ compounds have three-atom centered polyhedral structure: CuQ_4, MQ_6 and *Q* [(Ti,*M*)$_3$Cu]. As illustrated in Fig. 1, the chalcogen *Q* (*Q*=S, Se) atoms are coordinated by one copper and three metals to form *Q* [(Ti,*M*)$_3$Cu] tetrahedron. The distortion can be measured by the edge-length distortion (ELD) indices (see Table 4). The MQ_6 was slightly distorted (less than 3%), indicating a near-ideal octahedral structure. For all of the chalcospinel compounds, the *Q*[(Ti,*M*)$_3$Cu] tetrahedron was the most distorted polyhedron (~8% from the ideal tetrahedron). The CuQ_4 tetrahedra were ideal, with tetrahedral angles for the thio- and selenospinels of 109.5°.

Table 4
Edge length distortion Q–Q (Q=S or Se) of tetrahedral (ELD1) and Octahedral (ELD2) in $CuTi_{1.7}Mn_{0.3}S_4$(**I**), $CuTi_{1.7}Fe_{0.3}S_4$(**II**), $CuTi_{1.5}Fe_{0.5}S_4$(**III**), $CuTi_{1.7}Co_{0.3}S_4$(**IV**), $CuTi_{1.5}Co_{0.5}S_4$(**V**), $CuCr_{1.3}Ti_{0.7}Se_4$(**VI**), and $CuCr_{1.5}Ti_{0.5}Se_4$(**VII**).

	(I)	(II)	(III)	(IV)	(V)	(VI)	(VII)
ELD1[a] $Q[(Ti,M)_3Cu]$	7.95	7.94	7.94	7.94	7.94	7.94	7.95
ELD2[b] MQ_6	2.30	2.21	2.36	2.37	2.63	2.66	2.76

Where $(Q-Q)_i$ is chalcogen–chalcogen distance and $<Q-Q>$ is the average chalcogen–chalcogen distance of the edge in the polyhedron. M=Mn, Co, Fe or Cr.

[a] ELD1 $=\frac{100}{6}\sum_{i=1}^{6}\frac{(Q-Q)_i-<Q-Q>}{<Q-Q>}\%$.

[b] ELD2 $=\frac{100}{12}\sum_{i=1}^{12}\frac{(Q-Q)_i-<Q-Q>}{<Q-Q>}\%$.

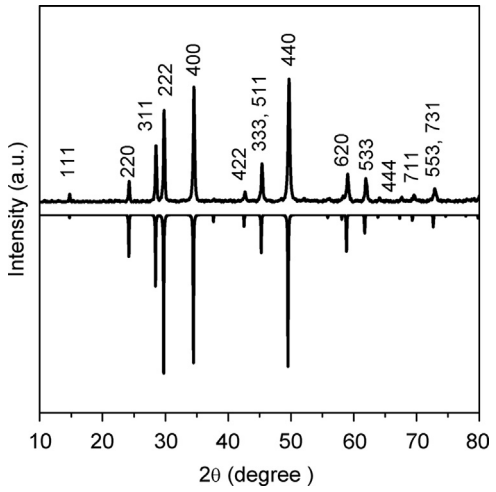

Fig. 2. The experimental X-ray powder diffraction pattern for $CuCr_{1.7}Ti_{0.3}Se_4$ (top) compared (in a mirror-like representation) to a simulated X-ray pattern from a single-crystal data (bottom).

3.2. Powder X-ray diffraction and SEM-EDAX

The XRD patterns were fully indexed in the space group $Fd\bar{3}m$ (N°227), providing evidence that the $CuTi_{2-x}M_xS_4$ and $CuCr_{2-x}Ti_xSe_4$ compounds have spinel-type structures. The experimental XRD patterns were compared with the simulated XRD patterns derived from the single-crystal XRD data. Fig. 2 shows a representative XRD pattern for $CuCr_{1.7}Ti_{0.3}Se_4$. The experimental XRD patterns for the $CuTi_{2-x}M_xS_4$ thiospinels are shown in Fig. 3. For the $CuCr_{2-x}Ti_xSe_4$ selenospinel series, the cell parameter a increased gradually as titanium was replaced by chromium (Table 5). The cell parameters obey Vegard's law. This can be explained by the lower ionic radii of Ti^{4+} as compared with Cr^{3+} ions. The octahedral ionic radii of Ti^{4+} and Cr^{3+} cations published by Shannon (for a high-spin configuration) are 0.605 Å and 0.615 Å, respectively. In contrast, for the $CuTi_{1.7}M_{0.3}S_4$ (M=Mn, Fe, Co) thiospinels, there is a reduction of the cell parameter a upon replacing Ti by the M metal, from Mn to Co (Table 5). The octahedral ionic radii (in HS configuration) of Mn^{2+}, $Fe^{2+}$and Co^{2+} are 0.83 Å, 0.78 Å and 0.745 Å, respectively. The chemical compositions of the powder samples were examined using EDAX analysis on polished surfaces of the pelletized samples (an example is shown in Fig. 4). The backscattered image and EDAX analysis (chemical maps of several areas) revealed that the samples were uniform throughout the scanned region (Table 5).

3.3. Magnetic measurements

The zero-field-cooled (ZFC)/field-cooled (FC) magnetization cycles for $CuCr_{2-x}Ti_xSe_4$ samples (x=0.3, 0.5 and 0.7), which were performed under low magnetic fields (500 Oe), are shown in Fig. 4.

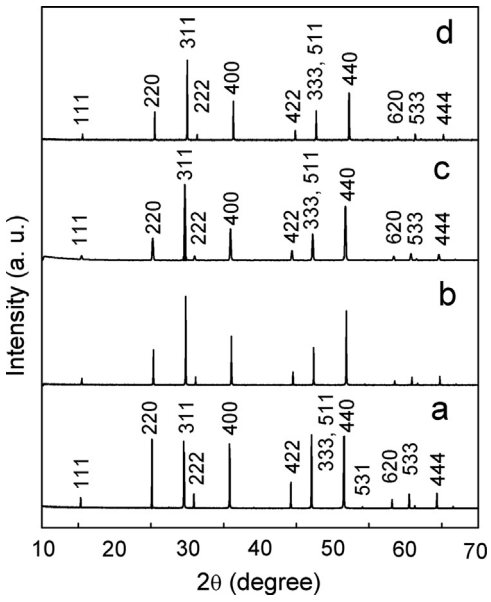

Fig. 3. Experimental X-ray powder diffraction patterns for (a) $CuTi_{1.7}Co_{0.3}S_4$, (b) $CuTi_{1.5}Fe_{0.5}S_4$, (c) $CuTi_{1.7}Fe_{0.3}S_4$ and (d) $CuTi_{1.7}Mn_{0.3}S_4$.

Table 5
Lattice parameters (XRD powder data) and chemical analytical data for thio- and seleno-spinel compounds.

Compound	Cell parameter a (Å)	Compositions from EDAX analyses
$CuCr_{2-x}Ti_xSe_4$		
x=0.7	10.421(2)	$Cu_{1.08}Cr_{1.32}Ti_{0.73}Se_{3.85}$
x=0.5	10.400(2)	$Cu_{1.03}Cr_{1.59}Ti_{0.52}Se_{4.10}$
x=0.3	10.373(2)	$Cu_{1.01}Cr_{1.77}Ti_{0.32}Se_{4.02}$
$CuTi_{2-x}M_xS_4$		
x=0.3; M=Mn	10.044(4)	$Cu_{0.98}Ti_{1.72}Mn_{0.25}S_{3.70}$
x=0.3; M=Fe	10.004(4)	$Cu_{0.99}Ti_{1.70}Fe_{0.26}S_{3.70}$
x=0.5; M=Fe	10.019(7)	$Cu_{1.02}Ti_{1.50}Fe_{0.47}S_{3.80}$
x=0.3; M=Co	9.935(4)	$Cu_{1.02}Ti_{1.66}Co_{0.28}S_{3.90}$
x=0.5; M=Co	9.898(5)	$Cu_{1.00}Ti_{1.58}Co_{0.50}S_{4.40}$

An evident ferromagnetic behavior is observed for all compounds, characterized by a high transition temperature T_C (Table 6) and large ZFC and FC ferromagnetic components. It is interesting to notice that the magnetization behavior in the ordered state is quite reversible because both the ZFC and FC modes were almost superimposed, except in the case of the chromium-richest sample ($CuCr_{1.7}Ti_{0.3}Se_4$), for which irreversible behavior started to occur almost at the transition temperature. It can be noticed from Fig. 5 that the ferromagnetic behavior is boosted by the substitution of Ti by Cr, reaching values of T_C well above room temperature for the richest sample in Cr (Table 6), making these materials very interesting for eventual applications. This trend is confirmed by a systematic increase in the positive Curie–Weiss temperature, which indicates the existence and further optimization of the ferromagnetic interactions.

The inset in Fig. 5 shows the inverse susceptibility of the $CuCr_{1.3}Ti_{0.7}Se_4$ compound, as measured in the paramagnetic regime under high applied fields (H_{app}=10 kOe). The inverse susceptibility, $1/\chi$, was fit with a classical Curie–Weiss relation $\chi=C/(T-\theta)$ in a temperature range that varied depending on the compound. As shown in Fig. 5, the corresponding range was 300 K $\leq T \leq$ 400 K, from which the effective moment μ_{eff} and the Curie–Weiss temperature θ were obtained (Table 6). The XAS analyses for the $CuCr_xTi_{2-x}Se_4$ selenospinel revealed that the titanium atoms were present in a 4+ oxidation state [19]. Nagata et al. proposed a model in which the Ti^{4+} ions were present in Cu

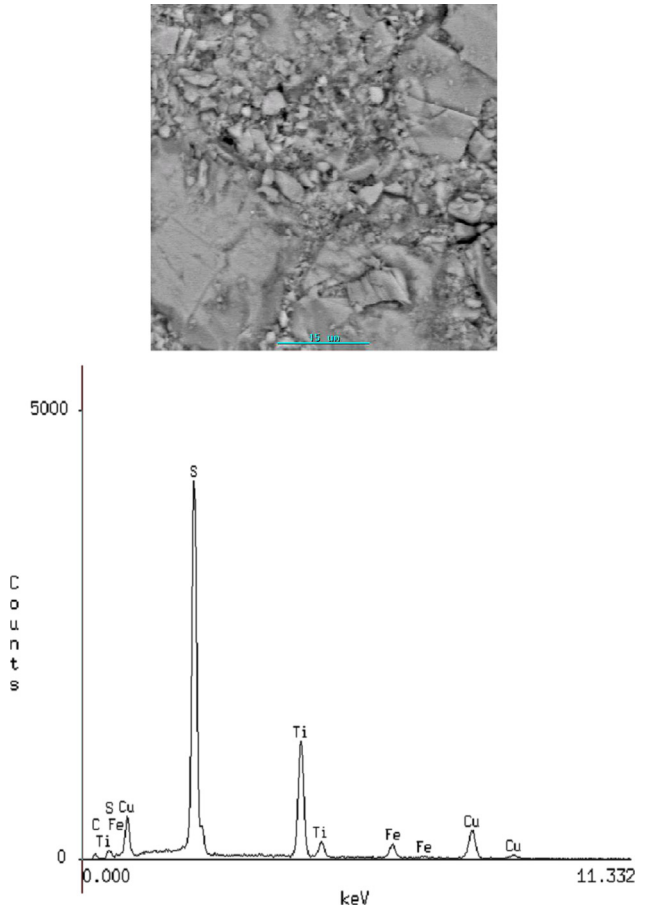

Fig. 4. Scanning electron microscopy (SEM) micrograph: Backscattering electron image of $CuTi_{1.7}Fe_{0.3}S_4$ (top) and an example of EDAX spectral analysis (bottom).

Table 6
Magnetic parameters for thio- and seleno-spinel compounds.

Compound	T_C[a],T_N[b](K)	μ_{eff} (μ_B)	θ (K)
$CuCr_{1.3}Ti_{0.7}Se_4$	165	4.29	+192
$CuCr_{1.5}Ti_{0.5}Se_4$	250	4.54	+275
$CuCr_{1.7}Ti_{0.3}Se_4$	332	4.96	+343
$CuFe_{0.3}Ti_{1.7}S_4$	6.7	2.64	−43
$CuFe_{0.5}Ti_{1.5}S_4$	8.7	3.51	−102
$CuMn_{0.3}Ti_{1.7}S_4$	–	3.19	−16.5
$CuCo_{0.3}Ti_{1.7}S_4$	–	0.54[c]	~0[c]
$CuCo_{0.5}Ti_{1.5}S_4$	–	0.58[c]	−8.7[c]

[a] T_C determined by extrapolation to the T-axis of the steepest slope of the FC magnetization.
[b] T_N corresponds to the temperature of the maximum of the susceptibility.
[c] Analyzed by a modified Curie–Weiss law, with TIP components.

$(Cr_xTi_{1-x})_2S_4$ cubic thiospinels [4]. In contrast, several experimental studies have suggested that the oxidation state of the copper is 1+ [31–35]. Assuming that the formal oxidation states of titanium and copper are 4+ and 1+, respectively, the oxidation state of the chromium ions will be 4+ and 3+. The observed effective moment for $CuCr_{1.3}Ti_{0.7}Se_4$ (μ_{eff}=4.29 μ_B) was close to the expected moment for high-spin states: $Cu^{1+}[\ Cr^{3+}_{1.0}Cr^{4+}_{0.3}]Ti^{4+}_{0.3}Se_4$ (μ^{theo}=4.17 μ_B).

The thiospinels studied in this work show quite different magnetic behaviors compared to the one discussed above. In the case of M=Co ($CuTi_{2-x}Co_xS_4$, x=0.3 and 0.5), a large temperature-independent paramagnetism (TIP) was observed. The magnetic susceptibilities were analyzed using a modified Curie–Weiss law of the type $\chi = C/(T-\theta)+\chi^{TIP}$. The TIP component, which was on the order of 380×10^{-6} (emu/mol), was evaluated from a [$\chi \times T$-*vs*-T] representation, as shown in the inset, Fig. 6. Their slopes allowed to evaluate a quite weak paramagnetic moment, which were on the order of 0.5 μ_B (Table 6), probably due to a small amount of Cu^{2+} present in the sample, with Co^{3+} in a low-spin non-magnetic state. Classical paramagnetic properties were observed for the Mn-doped sample, $CuTi_{1.7}Mn_{0.3}S_4$, that is, absence of long-range interactions, an effective moment of 3.19 μ_B and a negative Curie–Weiss temperature Θ_{CW} of the order of −16.5 K (Fig. 7).

Antiferromagnetic interactions were clearly observed for $CuTi_{2-x}Fe_xS_4$ (x=0.3 and 0.5). The paramagnetic state was measured under high applied fields (Fig. 8) at 100–300 K and was analyzed using the Curie–Weiss law to yield effective moments μ_{eff} of 2.64 μ_B and 3.51 μ_B for x=0.3 and x=0.5, respectively. The high values for the negative Curie–Weiss temperature Θ_{CW} (−42.7 K and −102 K for x=0.3 and 0.5, respectively) indicate that these compounds developed long-range antiferromagnetic interactions. Special attention should be paid to the $CuTi_{1.5}Fe_{0.5}S_4$ composition since magnetic frustration seems to be predominant. Indeed, as in all frustrated systems, the ratio $f(Q_{CW}/T_N)$, known as the frustration parameter, is a good indicator of the intensity of the magnetic frustration [36], for which values of f exceeding 10 constitute an accepted criterion to define magnetically frustrated systems. In the case of the x(Fe)=0.5 thiospinel studied in this work, such factor is of the order of 12. The inset in Fig. 8 shows the low-temperature

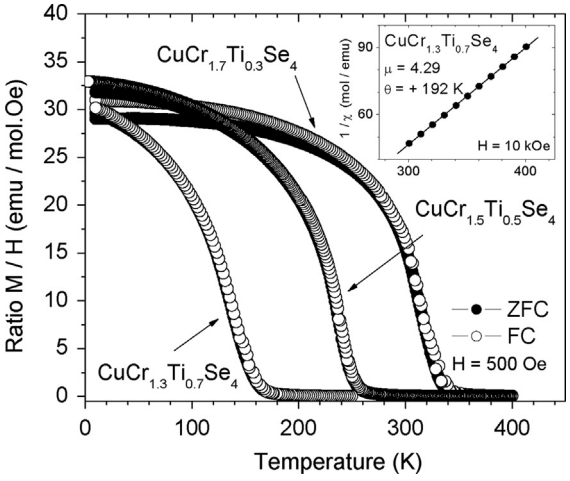

Fig. 5. Zero-field-cooled/field-cooled magnetization cycles at 500 Oe for pelletized powder samples of $CuCr_{1.3}Ti_{0.7}Se_4$, $CuCr_{1.5}Ti_{0.5}Se_4$ and $CuCr_{1.7}Ti_{0.3}Se_4$. The insert shows the $1/\chi$-*vs*-temperature behavior fitted by the Curie–Weiss law for $CuCr_{1.3}Ti_{0.7}Se_4$ at 10 kOe.

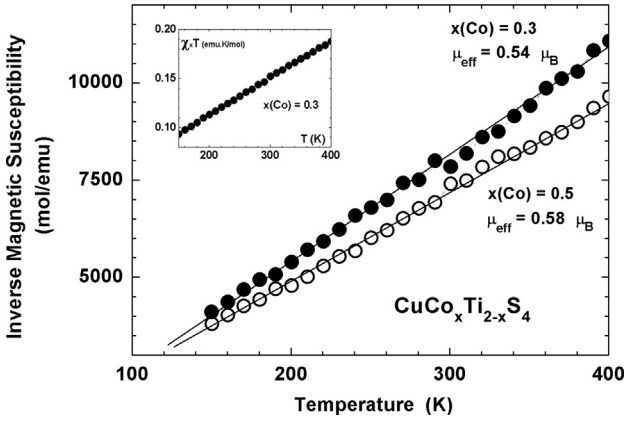

Fig. 6. Plot of the inverse values $(\chi-\chi^{TIP})^{-1}$, as a function of temperature. The insert shows the [$\chi \times T$-*vs*-T] representation.

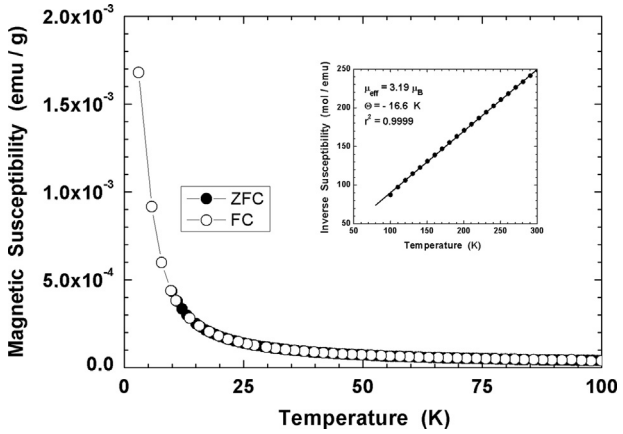

Fig. 7. Zero-field-cooled/field-cooled magnetization cycles of $CuTi_{0.7}Mn_{0.3}S_4$. The insert shows the $1/\chi$-*vs*-temperature behavior fitted by a Curie–Weiss law for $CuTi_{0.7}Mn_{0.3}S_4$ at 10 kOe.

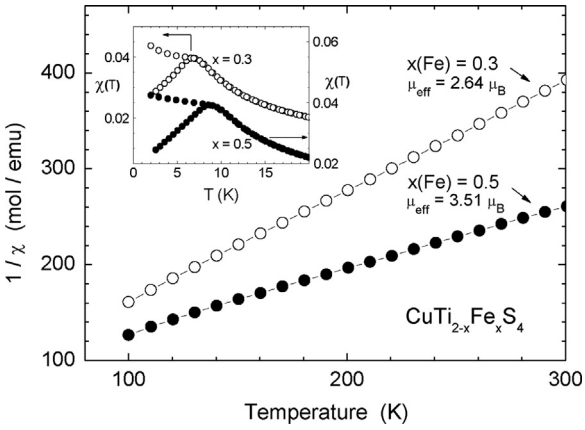

Fig. 8. The inverse magnetic susceptibility of $CuFe_{0.3}Ti_{1.7}S_4$ and $CuFe_{0.5}Ti_{1.5}S_4$, as analyzed by the Curie–Weiss law $\chi = C/(T-\theta)$. The inset shows the zero-field-cooled/field-cooled magnetization cycles measured at 1 kOe.

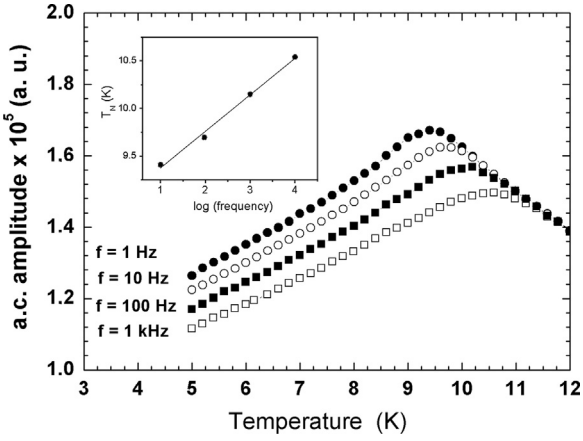

Fig. 9. a.c. Magnetic amplitude of $CuFe_{0.3}Ti_{1.7}S_4$. The inset shows the Neel T_N as a function of the frequency.

behavior of both compounds, as measured on ZFC/FC modes under an applied field of 1 kOe. Néel temperatures T_N of 6.7 K and 8.7 K, for $x=0.3$ and 0.5, respectively, were obtained, suggesting a spin-glass behavior. In order to confirm such behavior, a.c. susceptibility measurements were performed as a function of frequency. Fig. 9 illustrates the case of the $CuTi_{1.5}Fe_{0.5}S_4$ composition, showing a well-defined dependence of the maximum susceptibility with frequency, confirming that the Fe-doped thio-spinels are spin-glass materials. Table 6 shows the values of magnetic parameters for thiospinels studied in this work.

4. Conclusions

Single crystals of $CuTi_{1.7}Mn_{0.3}S_4$, $CuTi_{1.7}Fe_{0.3}S_4$, $CuTi_{1.5}Fe_{0.5}S_4$, $CuTi_{1.7}Co_{0.3}S_4$, $CuTi_{1.5}Co_{0.5}S_4$, $CuCr_{1.3}Ti_{0.7}Se_4$ and $CuCr_{1.5}Ti_{0.5}Se_4$ compounds were obtained by conventional solid-state synthesis. Their crystal structures, as determined by single-crystal X-ray diffraction, corresponded to spinel-type structures. The MQ_6 was slightly distorted (by less than 3%), indicating a near-ideal octahedral structure. For all of the chalcospinel compounds, the $Q[(Ti, M)_3Cu]$ tetrahedron was the most distorted polyhedron (~8% from an ideal tetrahedron).

The X-ray diffraction of the powder samples indicated that all of the phases crystallized in cubic spinel-type structures. The magnetic susceptibility measurements denoted ferromagnetic behavior for $CuCr_{2-x}Ti_xSe_4$ ($x=0.3$, 0.5 and 0.7). A cation oxidation-state model with Cu^+ and Ti^{4+} implied the presence of Cr^{3+} and Cr^{4+} cations, which explains the effective paramagnetic moments of the selenospinel $CuCr_{2-x}Ti_xSe_4$ materials.

The Co-based thiospinels, $CuTi_{1.7}Co_{0.3}S_4$ and $CuTi_{1.7}Co_{0.5}S_4$, showed a large temperature-independent paramagnetic contribution. Their effective moments (after subtraction of the TIP term) were quite weak (on the order of 0.5 μ_B), suggesting a small contribution from the divalent Cu in the samples. The Mn-based thiospinel $CuMn_{0.3}Ti_{1.7}S_4$ shows a paramagnetic behavior.

The Fe-based thiospinels ($CuTi_{1.7}Fe_{0.3}S_4$ and $CuTi_{1.5}Fe_{0.5}S_4$) show strong antiferromagnetic interactions, with relatively large negative Curie–Weiss temperatures and Néel temperatures T_N of 6.7 and 8.7 K, respectively, with a typical spin-glass behavior.

Acknowledgments

This work was supported by FONDECYT 1110161 and French-Chilean CNRS International Joint Laboratory LIA-MIF No 816. The authors are grateful to Vincent Dorcet, from CDIFX (Centre de Diffractométrie X, Université de Rennes 1, France) for the X-ray intensity data collections and Francis Gouttefangeas, from CMEBA (Centre de Microscopie Electronique, Université de Rennes 1, France) for SEM observations and EDAX analysis.

References

[1] L. Zhang, L. Ling, J. Fan, R. Li, S. Tan, Y. Zhang, J. Appl. Phys. 109 (2011) 113911.
[2] R. Masrour, M. Hamedoun, A. Benyoussef, J. Supercond. Nov. Magnet 24 (2011) 1729–1734.
[3] J. Krok-Kowalski, J. Warczewski, K. Krajewski, H. Duda, P. Gusin, T. Sliwinska, A. Pacyna, T. Mydlarz, S. Matyjasik, E. Malicka, A. Kita, J. Alloys Compd 430 (2007) 47–53.
[4] F. Kariya, S. Ebisu, S. Nagata, J. Solid State Chem. 182 (2009) 608–616.
[5] H. Okada, K Koyama, K. Watanabe, J. Alloys Compd 403 (2005) 34–37.
[6] G.J. Snyder, T. Caillat, J.-P. Fleurial, Mater. Res. Innovations 5 (2001) 67–73.
[7] P. Lavela, C. Pérez-Vicente, J.L. Tirado, C. Branci, J. Olivier-Fourcade, J.C. Jumas, Chem. Mater. 11 (1999) 2687–2693.
[8] H. Brändle, J. Schoenes, P. Wachter, F. Hulliger, W. Reim, Appl. Phys. Lett. 56 (1990) 2602.
[9] H. Brändle, J. Schoenes, P. Wachter, F. Hulliger, W. Reim, J. Magn. Magn. Mater. 93 (1991) 207.
[10] M. Robbins, H.W. Lehmann, J.G. White, J. Phys. Chem. Solids 28 (1966) 897.
[11] N. Soheilnia, K.M. Kleinke, E. Dashjav, H.L. Cuthbert, J.E. Greedan, H. Kleinke, Inorg. Chem. 43 (2004) 6473–6478.
[12] V.P. Sachanyuk, A.O. Fedorchuk, I.D. Olekseyuk, O.V. Parasyuk, Mater. Res. Bull. 42 (2007) 143–148.
[13] Zh. Kormosh, A. Fedorchuk, K. Wojciechowski, N. Tataryn, O. Parasyuk, Mater. Sci. Eng., C 31 (2011) 540–544.
[14] C. Branci, J. Sarradin, J. Olivier-Fourcade, J.C. Jumas, J. Power Sources 81–82 (1999) 282.
[15] R. Li, Z. Qua, L. Zhanga, L. Ling, W. Tonga, Y. Zhanga, Solid State Commun. 150 (2010) 2289–2293.

[16] V. Bodenez, L. Dupont, M. Morcrette, C. Surcin, D.W. Murphy, J.-M. Tarascon, Chem. Mater. 18 (2006) 4278–4287.
[17] F.K. Lotgering, R.P. Van Stapele, Solid State Commun. 5 (1967) 143.
[18] J.B. Goodenough, J. Phys. Chem. Solids 30 (1969) 261.
[19] H.-J. Noh, J.-S. Kang, S.S. Lee, G. Kim, S.-W. Han, S.-J. Oh, J.-Y. Kim, H.-G. Lee, S. Yeo, S. Guha, S.-W. Cheong, Europhys. Lett. 78 (2007) 27004.
[20] COLLECT, Software for CCD Diffractometers, Bruker AXS Inc, Madison, WI, USA, 1997–2004.
[21] A.J.M. Duisenberg, A.M.M. Schreurs, J. Appl. Crystallogr 36 (2003) 220.
[22] A.J.M. Duisenberg, R.W.W. Hooft, A.M.M. Schreurs, J. Kroon, J. Appl. Crystallogr 33 (2000) 893.
[23] SHELXL-97, Program for Solution and Refinement of Crystal Structures, Sheldrick GM, University of Göttingen, Germany, 1997.
[24] P. Pyykkö, Phys. Rev. B: Condens. Matter 85 (2012) 024115.
[25] G. Garg, S. Bobev, A.K. Ganguli, Solid State Ionics 146 (2002) 195–198.
[26] G. Garg, S. Bobev, A. Roy, J. Ghose, D. Das, A.K. Ganguli, Mater. Res. Bull. 36 (2001) 2429–2435.
[27] D. Skrzypek, E. Malicka, A. Waskowska, S. Widuch, A. Cichon, T. Mydlarz, J. Cryst. Growth 297 (2006) 419–425.
[28] W.H. Baur, Acta Crystallogr., Sect. B: Struct. Sci 30 (1974) 1195–1215.
[29] M. Wildner, Z. Kristallogr. 202 (1992) 51–70.
[30] K. Robinson, G.V. Gibbs, P.H. Ribbe, Science 172 (1971) 567–570.
[31] J.S. Bettinger, R.V. Chopdekar, M. Liberati, J.R. Neulinger, M. Chshiev, Y. Takamura, L.M.B. Alldredge, E. Arenholz, Y.U. Idzerda, A.M. Stacy, W. H. Butler, Y. Suzuki, J. Magn. Magn. Mater. 318 (2007) 65–73.
[32] D. Rodic, B. Antic, R. Tellgren, H. Rundlof, J. Blanusa, J. Magn. Magn. Mater. 187 (1998) 88–92.
[33] F.K. Lotgering, Proceedings of the International Conference on Magnetism, Nottingham (1964) 533.
[34] M. Robbins, H.W. Lehmann, J.G. White, J. Phys. Chem. Solids 28 (1967) 897.
[35] M. Gogolowicz, S. Juszczyk, J. Warczewski, T. Mydlarz, Phys. Rev. B: Condens. Matter 35 (1987) 7073–7080.
[36] P. Schiffer, A.P. Ramirez, Condens. Matter Phys. 18 (1996) 21.